Sustained Biexciton Populations in Nanoshell Quantum Dots

Journal:	*ACS Photonics*
Manuscript ID	ph-2019-00068h.R1
Manuscript Type:	Article
Date Submitted by the Author:	n/a
Complete List of Authors:	Kholmicheva, Natalia; Bowling Green State University, Physics Budkina, Darya; Bowling Green State University, Department of Chemistry Cassidy, James; Bowling Green State University Porotnikov, Dmitry; Bowling Green State University Harankahage, Dulanjan; Bowling Green State University Boddy, Anthony; Bowling Green State University, Center for Photochemical Sciences Galindo, Mireya; Saint Mary's University, Chemistry and Biochemistry Khon, Dmitriy; Saint Mary's University, Chemistry and Biochemistry Tarnovsky, Alexander; Bowling Green State University, Department of Chemistry Zamkov, Mikhail; Bowling Green State University,

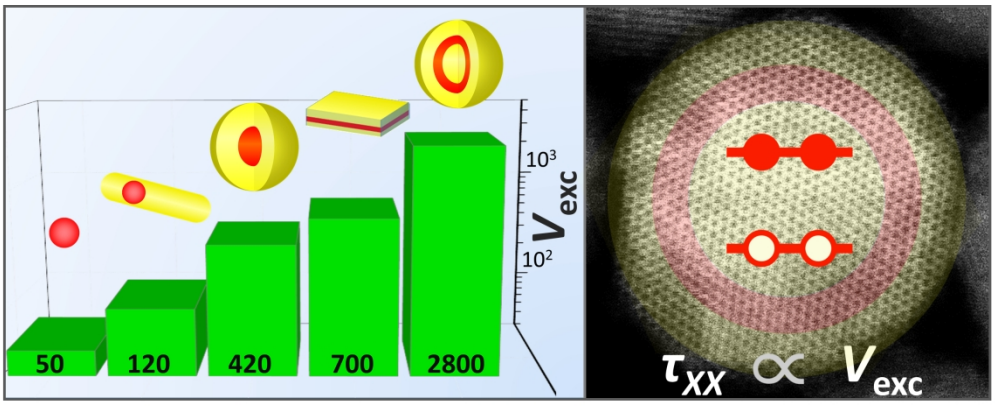

716x312mm (96 x 96 DPI)

Sustained Biexciton Populations in Nanoshell Quantum Dots.

Natalia Kholmicheva, [1,2] *Darya S. Budkina,* [1,3] *James Cassidy,* [1,2] *Dmitry Porotnikov,*[1,2] *Dulanjan Harankahage,*[1,2] *Anthony Boddy,*[1,2] *Mireya Galindo,*[4] *Dmitriy Khon,*[4] *Alexander N. Tarnovsky,*[1,3] *Mikhail Zamkov*[1,2,*].

The Center for Photochemical Sciences[1], Department of Physics[2] and Department of Chemistry[3], Bowling Green State University, Bowling Green, Ohio 43403. Department of Chemistry and Biochemistry[4], St. Mary's University, San Antonio, Texas, 78228.

Corresponding author: zamkovm@bgsu.edu; Tel: 419-372-0264; Fax: 419-372-9938

RECEIVED DATE (to be automatically inserted after your manuscript is accepted if required)

Keywords. Catalysis, photovoltaics, nanocrystals, biexcitons.

Abstract. Multiple exciton (MX) generation is beneficial to many applications of semiconductors, including photoinduced energy conversion, stimulated emission, and carrier multiplication. The utility of MX processes is generally enhanced in small-size semiconductor nanocrystals exhibiting the quantum confinement of photoinduced charges. Unfortunately, a reduced particle volume can also accelerate the non-radiative Auger decay of multiple

excitations, greatly diminishing the MX feasibility in nanocrystal-based photovoltaic, laser, and photoelectrochemical devices. Here, we demonstrate that such Auger recombination of biexcitons could be suppressed through the use of a quantum-well (QW) nanoshell architecture. The reported nanoscale geometry effectively reduces Coulomb interactions between photoinduced charges underlying Auger decay. This leads to increased biexciton lifetimes, as was demonstrated in this work through methods of ultrafast spectroscopy. In particular, we observed that the biexciton lifetime of CdSe-based QW nanoshells (CdS/CdSe/CdS) was increased more than thirty times relative to zero-dimensional CdSe NCs. The slower biexciton decay in QW nanoshells was attributed to a large confinement volume, which compared favorably to other existing MX architectures.

Multiple excitons (MX) play an important role in the photoinduced dynamics of semiconductor nanocrystals. The utilization of multiexciton effects in photovoltaic[1-3] and photoelectrochemical[4,5] devices has long been considered for converting the energy of a single high-energy photon into multiple carriers as a mechanism for mitigating thermal energy losses. Likewise, MXs are essential for the operation of quantum dot lasers,[6-9] where multiple excitons are required for achieving the excited-state population inversion, and was recently considered as a strategy for carrier concentration in multi-electron photocatalytic reactions (e.g. H_2 production, water oxidation).[10-13] The advancement of these applications faces an important challenge of overcoming the fast non-radiative Auger decay of multiple excitations in semiconductor nanocrystals.[7] This process is known to cause a reduced trion emission in nanocrystals and is often invoked to explain photoluminescence blinking in single quantum dots.[14] Even in the case of longer-lived biexciton populations (n = 2), the Auger decay time constant could be as short as just a few picoseconds (e.g. CdSe or PbSe NCs),[15,16] representing the predominant mechanism of carrier loss in laser and photovoltaic applications of these materials.[17,18]

Within the framework of Interacting Formalism,[19] the Auger recombination rate decreases linearly with the nanoparticle volume ($\Gamma^{-1} \sim V^{0.9\text{-}1.1}$).[20-24] As a result, the general solution for enhancing the biexciton lifetime of semiconductors is often sought through nanoscale geometries that offer a reduced confinement in one or two spatial dimensions. Along these lines, zero-dimensional nanocrystals have given way to architectures featuring mixed dimensionalities, such as alloyed core/shell nanoparticles,[25,26] nanorod-shaped heterostructures,[27-31] and nanoplatelets (NPLs),[32-34,35,36] where the increased confinement volume leads to long-lived biexcitons.

Quantum-Dot Quantum-Well (QDQW) systems[37-48] represent another example of low-dimensional colloids that could potentially result in suppressed Auger recombination of biexcitons. The quantum confined layer in these materials (e.g. CdSe, HgS) is sandwiched between the core and shell domains comprising a wider-gap semiconductor (e.g. CdS, ZnS). The resulting energy gradient leads to the formation of two-dimensional excitons that reside primarily in the intermediate shell and therefore exhibit an increased confinement volume. Recently, such quantum-well layers were successfully grown onto bulk-size core domains.[49,50] An important advantage of the bulk-seeded "nanoshell" geometry was associated with the ability to preserve the radial confinement of photoinduced charges regardless of the particle size. Consequently, all three dimensions of nanoshells could exceed the exciton Bohr radius enabling a significant increase in the exciton confinement volume.[49] The reported nanomaterials, however, employed a single-barrier CdS/CdSe architecture (Fig. SF1), where the carrier delocalization at unpassivated CdSe surfaces interfered with the biexciton dynamics.

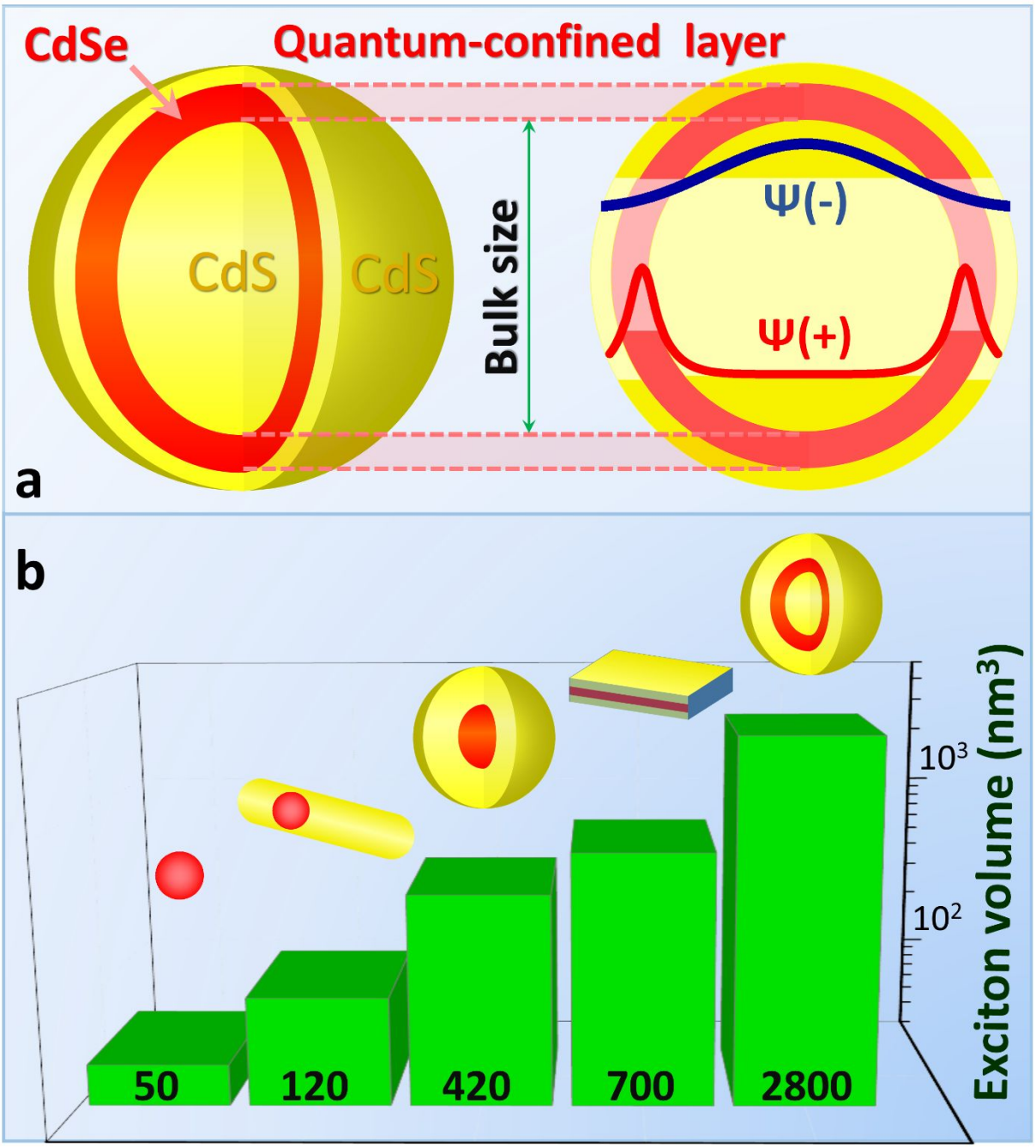

Figure 1. (a). Schematic illustration of a CdS_{bulk}/CdSe/CdS_{shell} quantum-well nanoshell geometry along with a projected carrier localization pattern. The energy offset of CdSe and CdS valence bands promotes a strong localization of photoinduced holes within the CdSe shell, meanwhile, the energetic proximity of electronic states in CdS_{bulk} and CdSe domains, as well as low effective

masses of CdS_{bulk} and CdSe electrons cause the delocalization of photoinduced electron wave functions over the entire nanocrystal volume. (b). An estimated quantum-confinement volume corresponding to several reported MX geometries. From left to right: spherical CdSe quantum dots (diameter = 4 nm), CdSe/CdS dot-in-a-rod (dot diameter = 4 nm, rod length = 30 nm), CdSe/CdS core/shell (core radius = 2 nm, shell radius = 10 nm), CdSe/CdS nanosheets (20 nm × 20 nm × 2nm), QW nanoshells, reported here (CdSe shell radius = 6 nm, shell thickness = 2 nm, total radius = 10 nm).

Here, we report on the synthesis of semiconductor quantum-well nanoshells exhibiting long-lived biexciton populations. The unique feature of the demonstrated nanoparticle architecture lies in the one-dimensional confinement of excitons within the surface layer (CdSe) of the bulk-size semiconductor nanoparticle (CdS_{bulk}). In this geometry (Fig. 1a), all three dimensions of CdS_{bulk}/CdSe/CdS_{shell} core/shell/shell nanostructures are allowed to exceed the exciton Bohr radius, lifting spatial limitations on the total particle size. We show that such arrangement of semiconductor domains allows increasing the volume of the carrier confinement more effectively than by using other zero-, one-, or two-dimensional geometries (Fig. 1b), which makes the reported architecture particularly suitable for suppressing Auger recombination processes. By using the femtosecond transient absorption spectroscopy, we demonstrate that the biexciton lifetime of CdS_{bulk}/CdSe/CdS_{shell} nanostructures featuring a 10-nm-diameter CdSe shell ($\tau_2 \approx 1.24$ ns) can be increased more than thirty times compared to that of zero-dimensional CdSe nanocrystals. The observed biexciton lifetime was found to be inversely proportional to the thickness of the quantum confined layer, which was attributed to the size-depended tuning of CdSe energy levels at CdSe/CdS interfaces. Our study has also revealed a significant contribution of surface recombination processes to single exciton decay in bulk-seeded nanoshells (quantum yield (QY) < 17%), as compared to similar processes in smaller-diameter QDQW (QY = 30-90%). Since the surface recombination could potentially affect the biexciton

dynamics on par with Auger processes, we believe that future improvements in the surface chemistry of these materials should result in further increases in the biexciton lifetime. Overall, the demonstrated suppression of Auger processes in $CdS_{bulk}/CdSe/CdS_{shell}$ nanoshells is expected to encourage the utilization of these nanostructures in MX applications (multiple exciton generation, stimulated emission), particularly since the reported geometry could be extended to a plethora of QDQW semiconductor combinations (e.g. CdS/HgS/CdS, ZnSe/InP/ZnSe, ZnS/CdS/ZnS). In addition to enhanced biexciton lifetimes, an important advantage of the nanoshell architecture includes a continuous density of excited states,[39,44,51] which permits lasing without the complete occupation of the CB edge,[52] similar to nanoplatelets[53,54] and nanosheets colloids.[55] Finally, a nearly spherical shape of nanoshells is expected to facilitate the assembly of these nanostructures into solids and superlattices,[56,57] a task which could be challenging in the case of non-spherical 1D and 2D colloids.

RESULTS AND DISCUSSION

Figure 1a shows a projected pattern of carrier confinement in $CdS_{bulk}/CdSe/CdS_{shell}$ quantum well nanoshells. A relatively high energy of the CdSe valence band (VB) edge is expected to result in a strong confinement of photoinduced holes within the CdSe domain.[58] In contrast, photoinduced electrons are likely to become delocalized over the entire nanoparticle volume due to nearly degenerate energies of conduction band (CB) edges in the two materials.[59] Under these conditions, the ensuing nature of electron-hole Coulomb interactions in QW nanoshells is strongly dependent on the relative offset of CB energies in CdS and CdSe semiconductors. If the global minimum of CB electrons lies in CdSe (type I confinement), the corresponding electron-hole spatial overlap will be greater than when such minimum is found in

the CdS material (quasi-type II confinement). Since the electron-hole overlap directly affects Coulomb interactions between photoinduced charges, the ultimate offset of CB energies in QW nanoshells should play an important role in determining the rate of corresponding Auger processes. To understand the magnitude of this effect, we have explored both aforementioned types of carrier confinement, which was accomplished by varying the thickness of the CdSe layer in $CdS_{bulk}/CdSe/CdS_{shell}$ QW nanoshells.

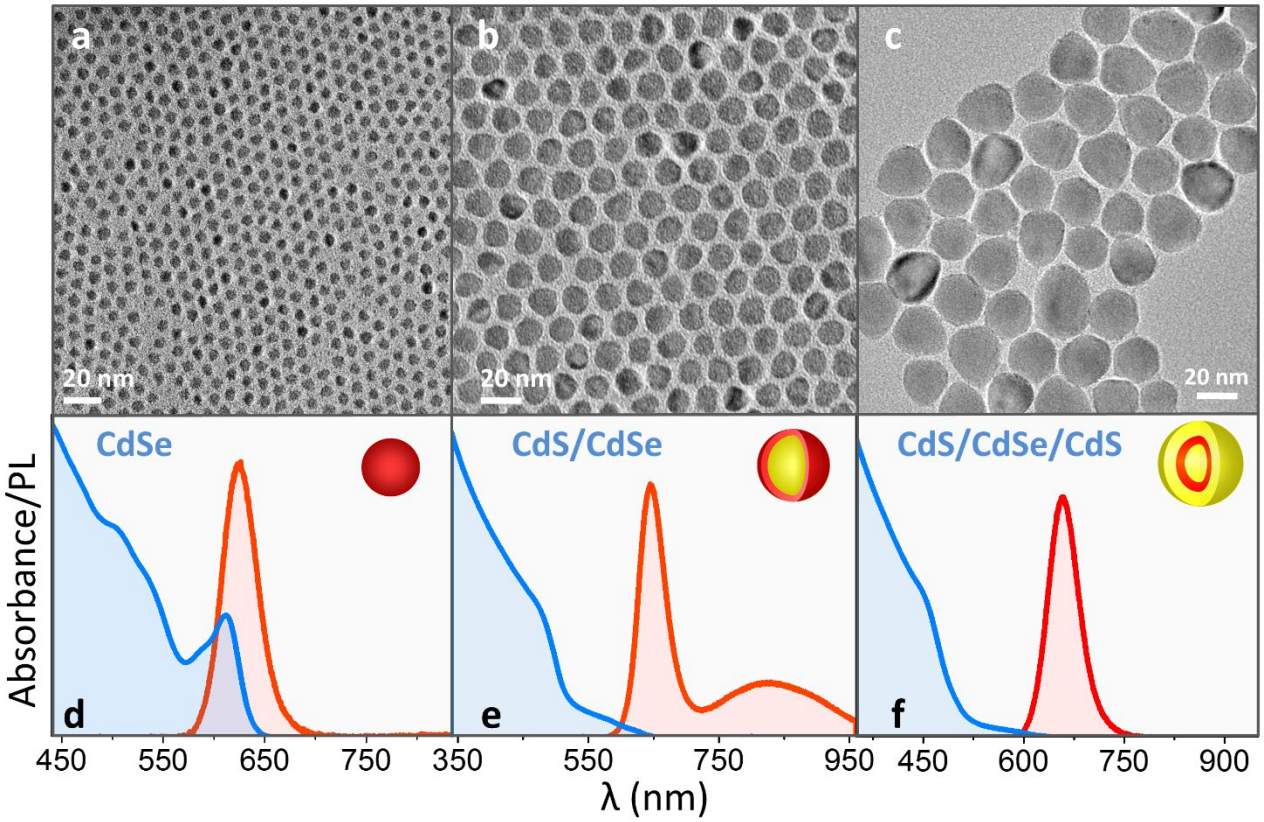

Figure 2. Characterization of three quantum-confined CdSe morphologies. (a). A TEM image of zero-dimensional CdSe nanocrystals (d ≈ 5.6 nm, see Fig. SF3a for the statistical size analysis). (b). A TEM image of 12.8-nm CdS/CdSe nanoshells featuring a 6.2-nm CdS core domain. (c). A TEM image of 23.8-nm $CdS_{bulk}/CdSe/CdS_{shell}$ QW nanoshells. (d-f). Emission and absorption profiles of three aforementioned CdSe morphologies, including (d). 5.6-nm CdSe NCs; (e).

CdS/CdSe nanoshells; and (f). 23.8-nm CdS_{bulk}/CdSe/CdS_{shell} QW nanoshells. The statistical analysis of size distributions is given in Fig. SF3.

CdS_{bulk}/CdSe/CdS_{shell} quantum well nanoshells were synthesized through a successive deposition of respective layers *via* hot-injection colloidal chemistry. First, bulk-size CdS nanoparticles (d = 5.8 - 13.1 nm) were grown by ripening 4-nm CdS nanocrystalline seeds in the presence of oleylamine.[60,61] The final product containing monodisperse, bulk-size CdS NCs, was then used for seeding the growth of the CdSe shell.[49] During the CdSe deposition stage, a mixture of Cd and Se precursors was gradually introduced into the solution of CdS_{bulk} nanoparticles. Slow injection speeds, controlled by a syringe pump, helped preventing the formation of isolated CdSe NCs. Typically, the shell growth was continued until the excitonic feature corresponding to the lowest-energy transition in the CdSe shell (λ = 550-630 nm) was observed in the absorption spectra (see Fig. 2e). The shoulder-like appearance of the exciton absorption profile in nanoshells was consistent with the two-dimensional character of the carrier confinement. The onset of the CdSe exciton absorption in CdS/CdSe nanoparticles was accompanied by the rise of the CdSe band gap photoluminescence (PL) signal, corresponding to the CB $\rightarrow$ VB carrier recombination in the shell domain (see Fig. 2e). In addition to the band-gap PL, the emission profile of CdS/CdSe nanoshells contained a broad spectral feature spanning the 700-1000 nm range, which was tentatively attributed to the interaction of "core" excitons with strongly coupled surface states.[62] We speculate that such surface emission in nanoshells could be enhanced relative to that of zero-dimensional CdSe NCs due to the surface localization of photoinduced holes (Fig. SF1a). Their strong interaction with the nanocrystal surface states could explain a relatively low, 1-3% PL quantum yield (QY) of the band gap emission in large-diameter (> 12 nm) CdS/CdSe nanoshell quantum dots. Conversely, Cd-$(oleate)_2$ capped small-diameter CdS/CdSe nanoshells were shown to exhibit the PL QY of up to 8%.[49]

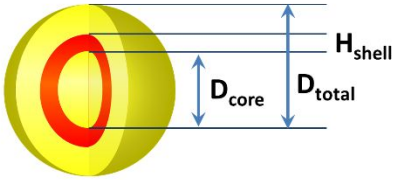

		D_{core} (nm)	H_{shell}(nm)	D_{total}(nm)	QY (%)	τ_{XX}(ns)	
1	**CdSe**			5.6	QY	**0.039**	
2	**CdS_{bulk}/CdSe**	13.1	2.7	18.4	1-2	**0.13**	
3	**CdS_{bulk}/CdSe**	6.2	3.3	12.8	2-3		
4	**CdS_{bulk}/CdSe**	5.8	1.9	9.6	4		
5	**CdS_{bulk}/CdSe/CdS_{shell}**	13.1	2.7	29.8	4	**0.41**	
6	**CdS_{bulk}/CdSe/CdS_{shell}**	13.1	2.7	24.9	8.7	**0.53**	
7	**CdS_{bulk}/CdSe/CdS_{shell}**	6.2	3.3	23.8	14	**0.85**	
8	**CdS_{bulk}/CdSe/CdS_{shell}**	5.8	1.9	16.2	17	**1.24**	

Figure 3. The summary of structural and optical parameters corresponding to 8 investigated samples. The sample number in the leftmost column is used as a unique sample ID in the results and discussion section.

Quantum-well nanoshells (CdS_{bulk}/CdSe/CdS_{shell}) were fabricated by growing a 3-5 nm CdS layer onto CdS/CdSe core/shell NCs. According to TEM images in Figs. 2b and 2c, the deposition of the CdS shell was evident through a significant increase in the particle diameter (see Fig. SF3 for the statistical analysis of particle size distributions). In all investigated QW nanoshell samples, summarized in Fig. 3, the CdS-shell growth step has resulted in the improved emission QY. Out of the two strategies for shell deposition, employing either the slow or fast[63] injection of precursors, the former method has yielded an overall better quality and a greater PL QY of QW nanoshells. Generally, the dispersion of CdS_{bulk}/CdSe/CdS_{shell} particle diameters was less than 10% (Fig. SF3c,e). On the contrary, the fast growth strategy has resulted in colloids

exhibiting a partly fragmented shell morphology with a corresponding particle size dispersion of 12.5% (Fig. SF4).

The growth of the CdS passivating layer on CdS/CdSe nanoshells was accompanied by the red-shift of the band gap emission (Fig. 2f) reflecting the delocalization of electronic wave functions into the CdS_{shell} domain. The quantum yield of the band gap PL in CdS_{bulk}/CdSe/CdS_{shell} nanoparticles has varied between 4 and 17% (Fig. 3) depending on the size of the CdS_{bulk} core and the quality of the CdS_{shell} layer. For instance, the highest QY value of 17% was observed for quasi-type II 16.2-nm QW nanoshells (sample 7, Fig. 3) featuring a 5.8-nm CdS core. Type I CdS_{bulk}/CdSe/CdS_{shell} nanostructures (Fig. 2c) comprising a similar core size (6.2 nm) yielded a QY of 14%. Overall, the brightness of the CdSe PL was generally lower for QW nanoshells containing larger-diameter CdS_{bulk} domain. According to Fig. 3, the QY of QW nanoshells comprising a 13.1-nm CdS_{bulk} core did not exceed 8.7%. The lower emissivity of QW nanoshells comprising a larger dimeter core could indicate a greater probability of non-radiative surface recombination in large-area CdSe. A possible lattice stress in the quantum-confined CdSe layer was identified as another potential factor contributing to non-radiative decay in QW nanoshells. According to x-ray powder diffraction (XRD) analysis of CdS_{bulk}/CdSe/CdS_{shell} nanoparticles in Fig. 4c (sample 4), only a single set of Bragg peaks, indexed to the wurtzite CdS crystallographic structure, was observed. Despite the absence of a distinguishable pattern corresponding to the CdSe diffraction, the asymmetric broadening of CdS peaks towards lower angles indicated the possibility of the CdSe lattice stress induced by the adjacent phases of the CdS_{core} and CdS_{shell} domains.

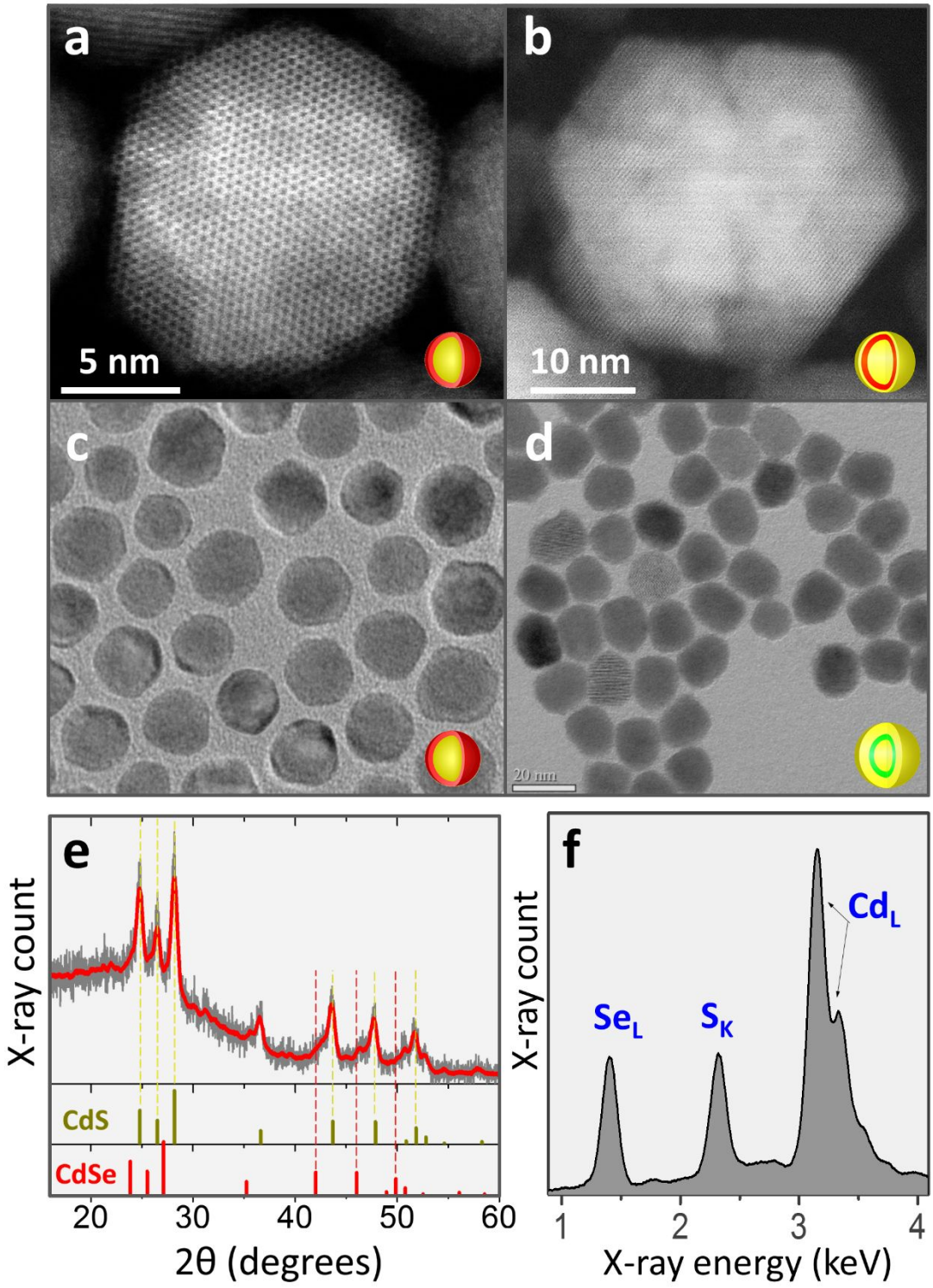

Figure 4. A high angle annular dark field (HAADF)-STEM image of (a) – a 12.8-nm CdS_{bulk}/CdSe nanoshell (sample 3 in Fig.3), and (b) – a CdS_{bulk}/CdSe/CdS_{shell} quantum-well nanoshell (sample 6). (c). TEM image of 18.4-nm CdS_{bulk}/CdSe nanoshells (sample 2)

comprising a 13.1-nm CdS core. (d). TEM image of 16.2-nm CdS_{bulk}/CdSe/CdS_{shell} quantum-well nanoshells (sample 8). (e). An x-ray powder diffraction (XRD) analysis of crystal phases in 18.4-nm CdS_{bulk}/CdSe nanoshells (sample 2), suggesting that core/shell nanoparticles grow in a wurtzite crystallographic phase a with CdSe domain exhibiting a stressed lattice pattern (peak broadening towards lower angles). (f). EDX analysis of elemental fractions in 18.4-nm CdS_{bulk}/CdSe nanoshells (sample 2).

Spectroscopic data combined with the TEM characterization of a nanoparticle product at different growth stages were used as the primary strategy for determining the thickness of the CdSe layer in CdS_{bulk}/CdSe/CdS_{shell} QW nanoshells. Ensuing CdSe-thickness assignments were found to be consistent with the Energy Dispersive X-ray (EDX) analysis performed on selected specimens. For instance, relative amplitudes of $S_{K\text{-}shell}$, $Se_{L\text{-}shell}$ and $Cd_{L\text{-}shell}$ x-ray signals in the 18.4-nm CdS/CdSe nanoshells (sample 2, Fig. 4f) suggest a 1:1.4 ratio of CdS to CdSe semiconductors in these nanoparticles, which falls within 10% of the CdS:CdSe ratio estimated from the TEM and UV-Vis analysis of the same structures (Figs. 4c and SF3b). The presence of the CdSe crystal phase in QW nanoshells was also confirmed by EDAX-STEM analysis of selected areas on a TEM grid (Fig. SF4).

The biexciton dynamics of nanoshell quantum dots was investigated by means of the femtosecond pump-probe transient absorption spectroscopy, as described in the experimental section. The laser pump wavelength (λ = 420 nm) was set to excite band gap transitions in both CdS and CdSe domains of nanoshells, which recovery was then probed using white-light supercontinuum (λ = 400-650 nm). The pump power was adjusted using neutral density filters to produce an average exciton population of $\langle N \rangle$ = 0.4-1.1 per single nanocrystal (see Fig. SF6).

To understand the effect of the radial carrier confinement in nanoshells on the ensuing biexciton dynamics, transient absorption (TA) measurements of CdS_{bulk}/CdSe/CdS_{shell} QW nanoshells were compared with those of zero-dimensional CdSe and unpassivated CdS_{bulk}/CdSe quantum dots. Figure 5b shows the chirp-corrected TA spectra of 5.6-nm CdSe NCs (sample 1). The excitation pulse resulted in photobleaching of the 1S(e)-$1S_{3/2}$(h) low-energy transition, denoted as $CdSe_{1S}$ ($\lambda \approx 610$ nm), as well as the higher-energy excitation, corresponding to the combination of 1S(e)-$2S_{1/2}$(h) and 1P(e)-$1P_{3/2}$(h) transitions[64] labelled A (λ = 500 - 540 nm). In the case of 18.4-nm CdS/CdSe nanoshells, TA spectra revealed two areas of photobleaching as indicated in Fig. 5e. A stronger ΔA signal at $\lambda \approx 500$ nm was attributed to the excitation-induced state filling of the 1S(e)-$1S_{3/2}$(h) transition in the CdS core, while the second TA bleach, observed at lower energies (λ = 540 – 610 nm), was attributed to the lowest-energy transition in the CdSe shell. Notably, the spectral position of the assigned CdSe bleach was correlated with the steady-state exciton absorption of the CdSe shell (Fig. 5d). In addition to the two negative ΔA signals, the TA spectra of both nanostructures contained derivative like distortions, labeled as B. The two signals had lifetimes comparable to those of 1S(e)-$1S_{3/2}$(h) transitions and were ascribed to their spectral interactions with the 1P(e) -$1P_{3/2}$(h) bands.[65,66] A slow recovery of the CdS bleach in CdS/CdSe nanoshells ($\lambda \approx 490$ nm, Figs. 5e and SF7) indicated the lack of a significant driving force for the photoinduced electron transfer into the CdSe shell. Indeed, due to the high degeneracy of hole levels in spherical CdS NCs, the TA bleach of band edge transitions is primarily contributed by electrons. Consequently, a slow reduction in the ratio of core-to-shell TA bleach amplitudes as a function of the pump-probe delay is consistent with the delocalization of the electron wave function over the entire nanoparticle volume.

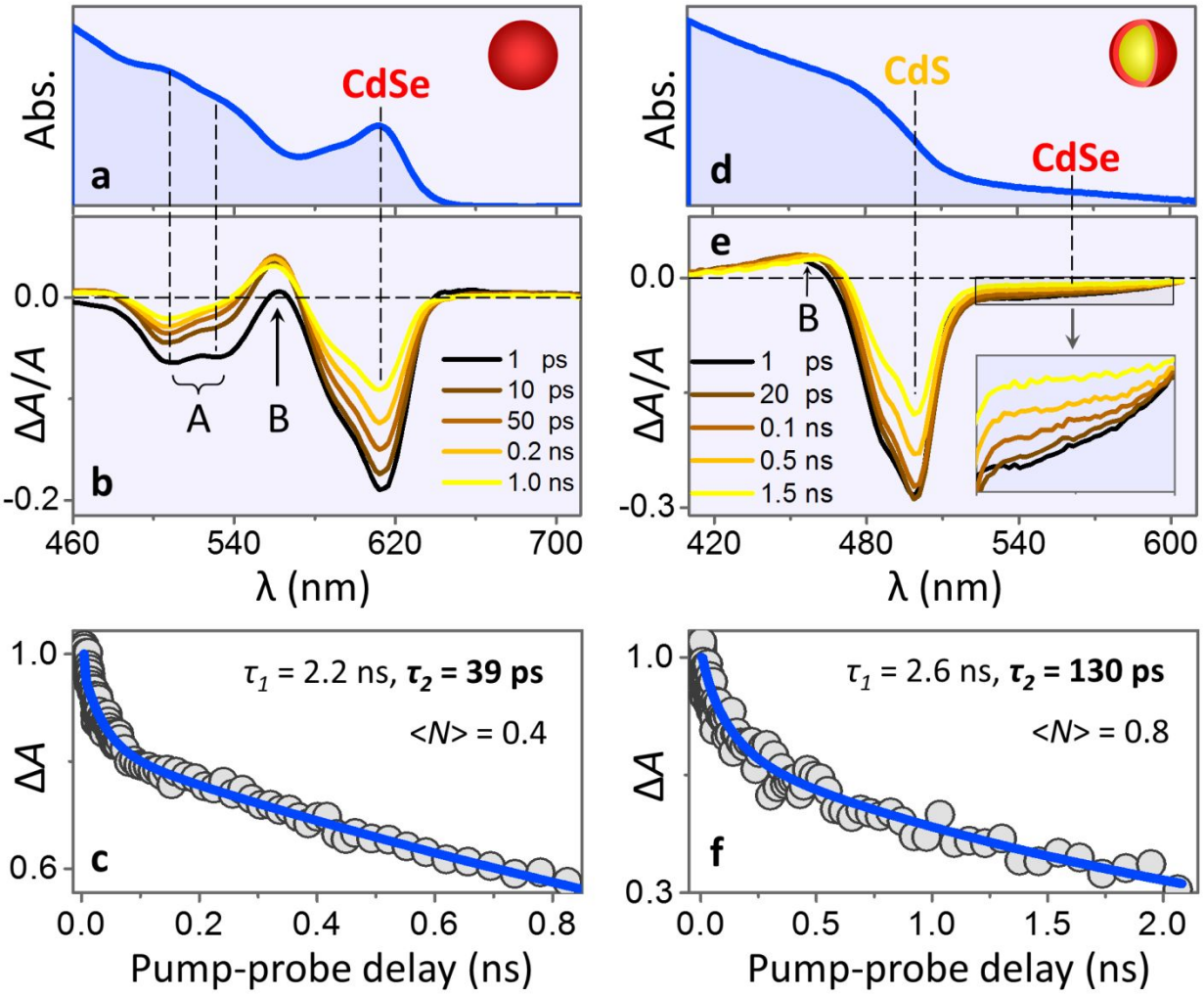

Figure 5. Measurements of biexciton lifetimes in zero-dimensional CdSe nanocrystals and CdS/CdSe nanoshells. (a). The absorption profile of 5.6-nm CdSe NCs. (b). The corresponding TA bleach recovery of the lowest energy $1S(e) \rightarrow 1S_{3/2}(h)$ transition. (c). The temporal evolution of the TA bleach, $\Delta A(1S)$, corresponding to lowest-energy transition in CdSe NCs is shown as circles. The experimental data was fitted using model calculations based on statistical scaling of Auger lifetimes and Poisson distribution of initial multi-exciton populations (Ref. 7). The biexciton lifetime was estimated to be τ_2 = 39 ps. (d). The absorption profile CdS/CdSe nanoshells showing the lowest-energy band gap transition in CdS_{bulk} and CdSe domains. (e). The corresponding TA bleach recovery of the lowest energy CB → VB transitions in CdS_{bulk} and CdSe. The TA dynamics of the CdSe spectral region is magnified in the insert. (f). The temporal evolution of the measured TA bleach associated with the CdSe shell (circles). The experimental

data was fitted using Eq. 1 resulting in the biexciton lifetime of τ_2 = 130 ps. The pump pulse fluence corresponded to <N> = 0.8 excitons per nanocrystal.

In order to extract biexciton lifetimes from the bleach recovery kinetics in Figs. 5c,f, we have employed the coupled rate equation formalism,[7] which assumes: (*i*) - Poisson distribution of initial multi-exciton populations in a nanocrystal ensemble, and (*ii*) - statistical scaling of Auger lifetimes. Within this strategy, the average number of photons absorbed by a nanoparticle, <N>, is first estimated from the known excitation pulse power, spectral density, and the sample absorption profile.[67] The average number of absorbed photons per particle is subsequently used to create the statistical distribution of nanoparticle fractions in the sample that receive n = 0,1,2 … excitons, $P(n)$. To this end, the probability of a nanocrystal absorbing n photons, $f(n)$, is assumed to follow the Poisson distribution: $f(n) = \langle N \rangle^n \times e^{-n} / n!$, as shown in Table ST1. Under the assumption that multiple excitons in a given nanocrystal decay sequentially (*via* the Auger recombination), the temporal evolution of the n-exciton population in a particle, $P(n, t)$, can be determined by solving coupled rate equations:

$$\frac{dP(n,t)}{dt} = \frac{P(n+1, t)}{\tau_{n+1}} - \frac{P(n,t)}{\tau_n} \quad (1)$$

where, τ_n represents the lifetime of the n-exciton state. The resulting evolution of multi-exciton populations, $P(n,t)$, obtained by solving Eq. 1, depends on a single unknown parameter, τ_2, corresponding to the Auger-limited biexciton lifetime. The single exciton lifetime, τ_1, as well as multi-exciton lifetimes (τ_n; n>2) entering Eq. 1 can be determined *a priori*. To this end, τ_1 is either extracted from the long-time TA bleach recovery at low excitation powers or obtained from the PL intensity decay (Fig. SF8). The lifetimes of multi-exciton states, τ_n, are computed using a statistical scaling law: $\tau_n^{-1} = n^2(n-1)\tau_2^{-1}/4$.[68] Owing to relatively low excitation powers used in present experiments ($\langle N \rangle \sim 1$), we assume that the TA bleach, ΔA, is contributed by up to four excitons, such that the average number of excitons per nanocrystal becomes,

$P(t) = 4 \times P(4,t) + 3 \times P(3,t) + 2 \times P(2,t) + P(1,t)$. The resulting parametric curve, $P(\tau_2, t)$, was used to fit the experimental measured TA bleach, ΔA(t), in order to determine the best fitting parameter, τ_2 (see Table ST1). We note that despite n = 2 being highest exciton occupation number for zero-dimensional CdSe NCs, due to a continuous electron density in CdS/CdSe nanoshells, these colloids are likely to support a larger number of band-edge excitons.

Figure 5c shows the TA bleach recovery kinetics for $CdSe_{1S}$ excitations in zero-dimensional CdSe nanocrystals. The best fit of the experimental data with the multi-exciton population curve, $P(t)$, has yielded the average biexciton lifetime of τ_2(CdSe) = 39 ps. In applying the fitting procedure, we have used the single exciton lifetime of τ_1(CdSe) = 2.2 ns, which was obtained from the double-exponential fit to the long-time TA data. The value of <N> = 0.4 was estimated from the excitation pulse fluence and further corroborated by the ΔA/A power dependence in Fig. SF6 (according to Ref. 20). Overall, the measured biexciton lifetime in 5.6-nm CdSe NCs appeared to be within the range of τ_2 reported by previous works.[69,70] Given the small size of these nanocrystals, the corresponding Auger decay was expected to be enhanced due to a strong interaction of photoinduced charges.

The multiexciton dynamics of CdS/CdSe nanoshells is analyzed in Fig. 5f, showing the temporal evolution of the integrated TA bleach recovery corresponding to the CB→VB transition in the CdSe shell. The experimental data was fitted with the multiexciton decay curve obtained by solving Eq. 1 (blue curve). In this case, a single exciton lifetime of τ_1 = 2.6 ns (see Table ST1) was obtained from the double-exponential fit to the long-time TA bleach recovery spectra. According to the best fit of the experimental data in Fig. 5f, the biexciton lifetime was determined to be τ_2 = 130 ps.

There are several processes that can potentially contribute to the decay of biexciton populations in CdS/CdSe nanoshells. In addition to the Auger recombination mechanism, multiple excitations could undergo a non-radiative decay through interactions with nanoshell surfaces, as their area is increased in comparison with zero-dimensional structures. Excitons can also funnel to the potential energy minimum of nanoshells associated with a locally enhanced CdSe thickness, where Coulomb interactions are increased. To estimate whether Auger recombination represents the primary process of biexciton decay, we have compared the volume dependence of measured biexciton lifetimes in CdS/CdSe and zero-dimensional CdSe NCs. Considering that the quantum-confinement volume of nanoshells, $V_{exciton}$, differs from the nanoparticle physical volume, the value of $V_{exciton}$ was obtained by using a strategy developed for alloyed-interface CdSe/CdS core/shell NCs.[26] The employment of the same model in characterizing photoinduced electrons of CdSe/CdS core/shell and CdS/CdSe nanoshell quantum dots could be reasonably expected due to the similarity of energy offsets and effective masses in bulk-like cores of nanoshells and bulk-like shells of CdSe/CdS nanocrystals. To this end, the effective volume was derived by using localization radii of the electron and hole wave functions, R_e and R_h, respectively, such that $V_{exciton} = (8\pi/3) \times (R_e^2)(R_h^2)/(R_e + R_h)$. The value of R_h for nanoshells was determined from the total volume of the shell V_{shell} as follows: $R_h = \sqrt[3]{(3/4\pi) \times V_{shell}}$). Accordingly, we estimate that for 18.4-nm nanoshells, $V_{exciton}$ is 9.8 times greater than the volume of 5.6-nm CdSe NCs, which places the biexciton lifetime in the 400 ps range. Consequently, the measured constant τ_2 = 130 ps falls short of the volume scaling prediction. The biexciton lifetime of nanoshells also appears shorter than Auger time constants reported for other two-dimensional forms of nanoscale CdSe, such as CdS/CdSe nanoplatelets (500 ps)[36] or alloyed-interface CdSe/CdS core/shell nanostructures (> 1 ns). A lower than

expected lifetime of biexcitons in CdS/CdSe nanoshells was tentatively attributed to the enhanced role of surfaces in a nanoshell geometry, where surface localized photoinduced holes can drive non-radiative recombination of excitons. The same issue could be responsible for a relatively short lifetime of single excitons in CdS/CdSe nanoshells ($\tau_1 \approx 2.2$ ns, see Table ST1).

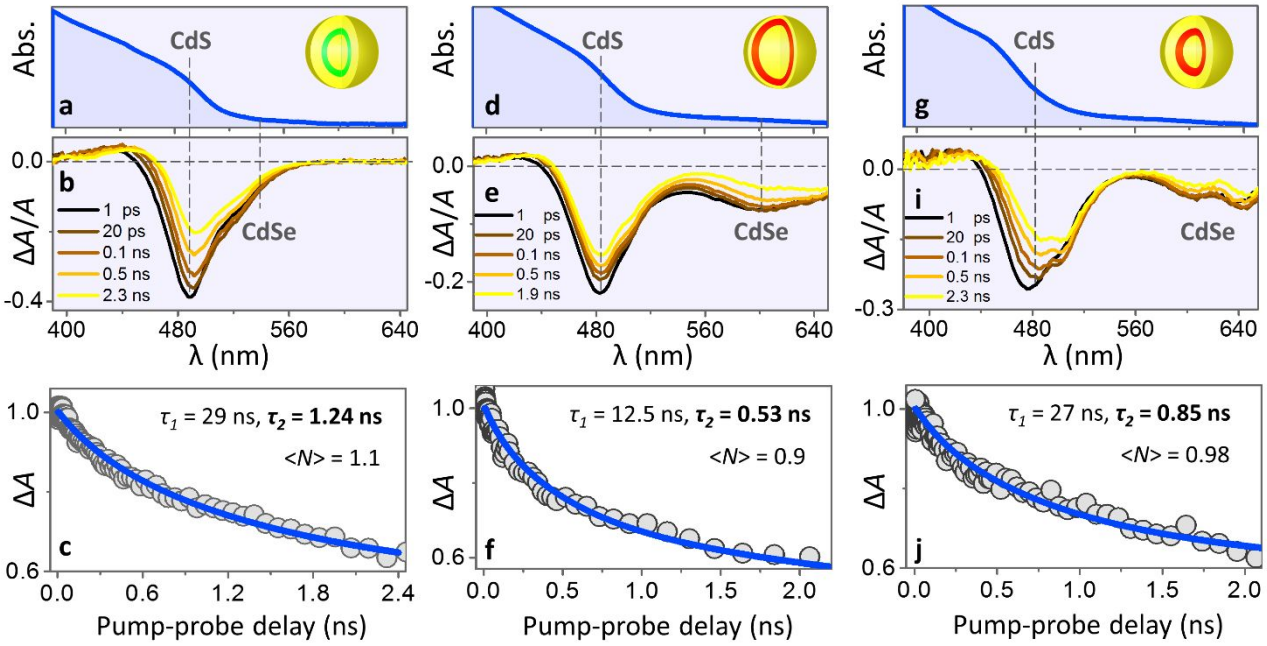

Figure 6. Measurements of biexciton lifetimes in $CdS_{bulk}/CdSe/CdS_{shell}$ quantum well nanoshells. (a). The absorption profile of 16.2-nm $CdS_{bulk}/CdSe/CdS_{shell}$ NCs (sample 8). (b). The corresponding TA bleach recovery spectra showing the low-energy transitions in CdS and CdSe domains. The pump fluence corresponded to an average of <N> = 1.1 photons per nanocrystal. (c). The temporal evolution of the TA bleach corresponding to CdSe shell excitons in 16.2-nm $CdS_{bulk}/CdSe/CdS_{shell}$ NCs (circles). The best fit of the experimental data based on Eq. 1 revealed the biexciton lifetime of τ_2 = 1.24 ns. (d). The absorption profile of 24.7-nm $CdS_{bulk}/CdSe/CdS_{shell}$ NCs (sample 6). (e). The corresponding TA bleach recovery spectra (<N> = 0.9 photons per nanocrystal). (f). The temporal evolution of the CdSe TA bleach recovery in 24.7-nm $CdS_{bulk}/CdSe/CdS_{shell}$ NCs (circles). The best fit of the experimental data corresponded to the biexciton lifetime of τ_2 = 530 ps. (g). The absorption profile of 23.9-nm

CdS_{bulk}/CdSe/CdS_{shell} NCs (sample 7). (i). Corresponding TA bleach recovery spectra (<N> = 0.98). (j). The temporal evolution of the CdSe TA bleach recovery in 23.8-nm CdS_{bulk}/CdSe/CdS_{shell} NCs (circles). The best fit of the experimental data corresponds to the biexciton lifetime of τ_2 = 850 ps.

The surface-induced carrier recombination in CdS_{bulk}/CdSe nanoshells was significantly reduced upon the deposition of the CdS_{shell} layer. The successful neutralization of surface traps in CdS_{bulk}/CdSe/CdS_{shell} QW nanoshells was evidenced through the enhancement in the PL quantum yield (from 1-3% to 17%) as well as an apparent increase in the single exciton lifetime (Fig. SF8). The presence of the "hole-blocking" surface layer in CdS_{bulk}/CdSe/CdS_{shell} nanostructures has also given rise to characteristic temporal changes in the TA dynamics of CdSe excitons, as summarized in Fig. 6. For all three investigated geometries of CdS_{bulk}/CdSe/CdS_{shell} QW nanoshells, including small-core type II (Fig. 6b), large-core type I (Fig. 6e), and small-core type I (Fig. 6i) specimens, the recovery of biexciton populations was noticeably slower than in the case of "unpassivated" CdS/CdSe nanoshells (Fig. 5e). According to the model fit of the integrated CdSe TA signal, small-core type II CdS_{bulk}/CdSe/CdS_{shell} QW nanoshell geometry resulted in the longest biexciton lifetime of τ_2 = 1.24 ns (Fig. 6c). A somewhat lower decay constant was observed for small-core type I nanostructures (τ_2 = 0.85 ns, Fig. 6j), exhibiting a stronger carrier overlap. The comparison of the TA bleach recovery between type I (sample 7) and type II (sample 8) QW nanoshells has help identifying the effect of the carrier localization on the value of τ_2, as both specimens featured nearly the same CdS_{bulk}/CdSe/CdS_{shell} and CdS_{bulk} diameters (see Fig. 3). As indirect evidence supporting the type I carrier localization assignment in sample 7, we have observed a rise in the $\Delta A(CdSe)/\Delta A(CdS)$ ratio with increasing pump-

probe decay (Fig. SF7). The fast growth of this ratio at early times was consistent with the transfer of excitations from the CdS domain (both CdS_{bulk} and CdS_{shell}) into the CdSe layer.

The observation of a shorter biexciton time constant for type I QW nanoshells (sample 7) was consistent with a relatively smaller exciton volume in these nanostructures. Furthermore, in comparison with type I core/shell nanocrystals, the type II localization regime has been predicted to increase the repulsive component of the Coulomb interaction causing a net repulsion of biexcitons,[71] thus diminishing their corresponding Auger recombination rates. Such an enhancement of the biexciton lifetime in type II structures has been also observed in CdSe/CdS core/shell and ZnSe/CdSe core/shell nanostructures.[71,72] Finally, samples featuring a large-size CdS core yielded the lowest of three biexciton lifetimes, τ_2 = 0.53 ns. While the exciton volume for this QW geometry was greater than in the case of small-core type I nanocrystals (sample 7), the single exciton lifetime for large-core nanoshells was comparatively low (τ_1 = 12.5 ns, Fig. 6f). This was likely the result of enhanced surface recombination caused by a relatively large surface area of the quantum-confined CdSe. As was stated above, the synthesis of such large-core QW nanoshells has not been optimized to the same degree as for small-core nanostructures. We expect, however, that with the future improvements in the surface passivation of large-core nanoshells, the biexciton time constant could be increased beyond the range of τ_2 reported for small-core structures.

CONCLUSIONS

In conclusion, we report on the synthesis of semiconductor quantum-well nanoshells exhibiting long-lived biexciton populations. The demonstrated nanoparticle architecture utilizes a CdS_{bulk}/CdSe/CdS_{shell} core/shell/shell morphology, which effectively reduces the rate of Auger

recombination in the quantum-confined layer of CdSe. As a result, the non-radiative decay of biexcitons becomes suppressed, as was demonstrated in this work by means of the femtosecond transient absorption spectroscopy. In particular, we show that the biexciton lifetime of $CdS_{bulk}/CdSe/CdS_{shell}$ nanostructures featuring an 8-nm-diameter CdSe shell ($\tau_2 \approx 1.24$ ns) was increased more than thirty times compared to that of zero-dimensional CdSe nanocrystals. We expect that the demonstrated QW nanoshell architecture could useful in applications where long-lived biexciton populations are critical to performance. Furthermore, a nearly spherical shape of QW nanoshells is expected to facilitate the assembly of these nanostructures into solids and superlattices, a task, which could be challenging in the case of non-spherical 1D and 2D colloids.

METHODS.

Materials. The following materials were used: cadmium oxide (CdO, 99% Aldrich), 1-octadecene (ODE, 90% Aldrich), oleic acid (OA, 90% Aldrich), sulfur (S, 99.99% Acros), ethanol (anhydrous, BeanTown Chemical), chloroform (anhydrous, 99% BeanTown Chemical), oleylamine (OLAM, tech., 70% Aldrich), tri-n-octylphosphine (TOP, 90% Acros), tri-n-octylphosphine oxide (TOPO, 99.0% Aldrich), selenium powder (Se, 200 mesh, Acros), acetone (anhydrous, Amresco, ACS grade), All reactions were performed under argon atmosphere using the standard Schlenk technique. The centrifuge (VWR Clinical 100) used for precipitation operated at 6500 rpm.

Synthesis of CdS bulk-size nanocrystals. Bulk-size CdS nanocrystals (d= 6 - 14 nm) were fabricated through digestive ripening of small-diameter CdS nanocrystals prepared according to Ref. 73. The details of the digestive ripening protocol are given in Ref. 60. Briefly, small-diameter CdS NC seeds were transferred into a flask containing a mixture of OLAM:ODE = 60:40 (total volume is 7 mL) and degassed at 120 °C to remove chloroform. The reaction mixture was subsequently heated to 260 °C under argon. When the desired nanoparticle size was reached, the reaction was stopped by removing the flask from the heating mantle. The NC

product was separated from the solution by precipitating with acetone and redispersing in chloroform.

Synthesis of CdS/CdSe nanoshells. The deposition of the CdSe shell onto bulk-like CdS nanoparticles was performed using a previously reported strategy.[49] First, cadmium oleate was prepared by dissolving 0.025 g of CdO in the mixture of 0.4 ml of OA and 5.4 mL of ODE under argon flow at 260 °C and cooled down to room temperature. In a separate flask, 0.015 g of Se was dissolved in 1 mL of TOP at 120 °C. The TOP-Se mixture was added to Cd-$(oleate)_2$ at room temperature. For the CdSe shell deposition, the reaction mixture containing bulk-size CdS NCs in chloroform, 4 ml of OLAM, and 10 ml of ODE was degassed at 120 °C, switched to argon, and heated to 260 °C. When the temperature stabilized the combined precursor mixture was injected into the reaction flask *via* a syringe pump at a rate of 1 mL/h. Once the desired CdSe shell size was reached (typically, when the intensity of the CdSe shell PL became prominent), the reaction was stopped by removing the flask from the heating mantle. The product was separated from the solution by precipitation with ethanol/acetone mixture (1:2) and was stored in chloroform.

Synthesis of CdS_{bulk}/CdSe/CdS_{shell} quantum well nanoshells. The growth of the CdS passivating layer on CdS/CdSe nanoshells was performed according to either Cirillo *et al*.[63] or Jeong et al.[74] methodology. The latter method yielded an overall better-quality nanocrystals exhibiting a relatively greater QY. In this case, cadmium oleate was prepared by degassing a mixture of 0.034 g of CdO, 0.8 ml of OA, and 5 ml of ODE at 120° C for 30 min followed by switching the flask to argon atmosphere and heating to 230° C until solution turned clear. At the same time, a mixture of 0.026 g of S powder and 1.8 ml of TOP was degassed at 120°C for 30 min. Both Cd and S precursors were mixed at room temperature and stored under argon flow. For the CdS shell deposition, a mixture of CdS/CdSe seeds in chloroform, 4 ml of OLAM, and 10 ml of ODE was transferred to the reaction flask and degassed at 120°C for 1 hour. Subsequently, the flask was switched to Ar and heated to 260°C. As soon as the temperature stabilized, the Cd/S precursor mixture was injected into the flask with the syringe pump at a rate of 2 mL/h. Once the desired shell size was reached, the reaction was stopped by removing the flask from the heating mantle. The product was separated from the solution by precipitation with ethanol/acetone mixture (1:2) and was stored in chloroform.

Characterization. UV-vis absorption spectra were recorded using a CARY 60 scan spectrophotometer. High resolution transmission electron microscopy (TEM) measurements were carried out using JEOL JEM-3011UHR operated at 300 kV. Specimens were prepared by depositing a drop of NP solution in organic solvent onto a carbon-coated copper grid and allowing it to dry in air. Powder X-ray diffraction measurements were carried out with a Bruker D8 Advance PXRD. Luminescence spectra where acquired using a 400-nm PicoQuant PDL 800-D pulsed laser and measured with an Andor newton^{EM} detector. Time-resolved emission lifetime spectra where acquired using the same 400-nm pulsed laser and photons where collected and processed using a SPC-130 TCSPC module from Boston Electronics. Relative quantum yield measurements where acquired using a GS32 Intelite 532-nm CW DPSS laser (Cyanine3 NHS ester dye obtained from Lumiprobe was used as the reference).

Transient Absorption Measurements. The femtosecond transient absorption spectrometer used in these experiments is based on a regeneratively amplified Ti:Sapphire laser system (Hurricane, Spectra-Physics) that generates a 1-kHz train of 90 fs (fhwm), 0.9 mJ/pulses centered at 800 nm. The amplified beam is 50:50 split. The first beam is sent to a TOPAS-C optical parametric amplifier to produce 420 nm (or, 500 nm) pulses used for sample excitation. The second beam is attenuated, sent through a computer-controlled optical delay stage, and then focused onto a 3-mm CaF_2 window to produce a white-light continuum (wlc) probe spanning the 345-760 nm range. The wlc probe beam was focused to a 75 μm diameter spot at the sample position and overlapped at a 6° angle with the excitation beam focused to a 150 μm diameter spot. A fraction of the wlc probe beam was split off before the sample to be utilized as a reference for the correction of shot-to-shot pulse-intensity fluctuations. The probe (after the sample) and reference beams were dispersed by a spectrograph and recorded using a dual 512-pixel diode array detector synchronized to the 1-kHz repetition rate. The difference between the decadic logarithms of a probe-to-reference pulse intensity ratio was measured at a specific position of the optical stage for the case when excitation pulse was on and off. Typically, 300 on and off pairs were averaged to produce the transient absorption signal (ΔA) at the corresponding delay time, and then the procedure was repeated for about 10 scans of the optical delay stage. The solutions were kept in a 1-mm path length cell or in a spinning 2 mm path length cuvette. These two sets of conditions did not have any noticeable difference on time and spectral evolution of transient absorption signals. The zero delay time positions at different probe wavelengths were obtained from non-

resonant electronic responses from neat $CHCl_3$ solvent measured at the same experimental conditions,[75] and used for the chirp correction of the measured ΔA data. The typical excitation energy was 0.5 μJ/pulse. The linearity of ΔA signals with excitation energy confirmed that single-photon excitation is responsible for the measured data. The polarization of the excitation beam was set at the magic angle (54.7°) with respect to the probe beam to eliminate signals from rotational dynamics of the solute. All experiments were performed at 21 °C.

Supporting information. Experimental section, additional figures and details of calculation. This material is available free of charge via the Internet at http://pubs.acs.org.

Acknowledgment. This work was supported by the Award DE-SC0016872 (MZ) funded by the U.S. Department of Energy, Office of Science. MG was funded by the Welch foundation grant # U-0047. A.N.T. acknowledges the support from NSF (CHE-0923360 and CHE-1626420).

REFERENCES

[1] Sukhovatkin, V.; Hinds, S.; Brzozowski, L.; Sargent, E. H. Colloidal quantum-dot photodetectors exploiting multiexciton generation. *Science* **2009***, 324*, 1542-1544.

[2] Semonin, O. E.; Luther, J. M.; Choi, S.; Chen, H.; Gao, J.; Nozik, A. J.; Beard, M. C. Peak external photocurrent quantum efficiency exceeding 100% via MEG in a quantum dot solar cell. *Science* **2011***, 334*, 1530-1533.

[3] Nair, G.; Chang, L.; Geyer, S. M.; Bawendi, M. G. Perspective on the prospects of a carrier multiplication nanocrystal solar cell. *Nano Lett.* **2011***, 11*, 2145-2151.

[4] Yan, Y.; Crisp, R. W.; Gu, J.; Chernomordik, B. D.; Pach, G. F.; Marshall, A. R.; Turner, J. A.; Beard, M. C. Multiple exciton generation for photoelectrochemical hydrogen evolution reactions with quantum yields exceeding 100%. *Nat. Energy* **2017***, 2*, 17052.

[5] Zamkov, M. Solar hydrogen generation: Exceeding 100% efficiency. *Nat. Energy* **2017***, 2*, 17072.

[6] Klimov, V. I. Spectral and dynamical properties of multiexcitons in semiconductor nanocrystals. *Annu.Rev.Phys.Chem.* **2007***, 58*, 635-673.

[7] Klimov, V. I.; Mikhailovsky, A. A.; Xu, S.; Malko, A.; Hollingsworth, J. A.; Leatherdale, a. C.; Eisler, H.; Bawendi, M. G. Optical gain and stimulated emission in nanocrystal quantum dots. *Science* **2000***, 290*, 314-317.

[8] Yang, Z.; Pelton, M.; Fedin, I.; Talapin, D. V.; Waks, E. A room temperature continuous-wave nanolaser using colloidal quantum wells. *Nat. Commun.* **2017***, 8*, 143.

[9] Kambhampati, P. Multiexcitons in Semiconductor Nanocrystals: A Platform for Optoelectronics at High Carrier Concentration. *J. Phys. Chem. Lett.* **2012**, *3*, 1182– 1190.

[10] Blankenship, R. E.; Tiede, D. M.; Barber, J.; Brudvig, G. W.; Fleming, G.; Ghirardi, M.; Gunner, M. R.; Junge, W.; Kramer, D. M.; Melis, A. Comparing photosynthetic and photovoltaic efficiencies and recognizing the potential for improvement. *Science* **2011***, 332*, 805-809.

[11] Lewis, N. S.; Nocera, D. G. Powering the planet: Chemical challenges in solar energy utilization. *Proc. Natl. Acad. Sci. U. S. A.* **2006***, 103*, 15729-15735.

[12] Kholmicheva, N.; Royo Romero, L.; Cassidy, J.; Zamkov, M. Prospects and applications of plasmon-exciton interactions in the near-field regime. *Nanophotonics* **2018**, DOI: https://doi.org/10.1515/nanoph-2018-0143.

[13] Moroz, P.; Boddy, A.; Zamkov, M. Challenges and Prospects of Photocatalytic Applications Based On Semiconductor Nanocrystals. *Front. Chem.* **2018**, *6*, 353.

[14] Nirmal, M.; Dabbousi, B. O.; Bawendi, M. G.; Macklin, J. J.; Trautman, J. K.; Harris, T. D.; Brus, L. E. Fluorescence intermittency in single cadmium selenide nanocrystals. *Nature* **1996***, 383*, 802.

[15] Klimov, V. I.; McGuire, J. A.; Schaller, R. D.; Rupasov, V. I. Scaling of multiexciton lifetimes in semiconductor nanocrystals. *Phys. Rev. B* **2008***, 77*, 195324.

[16] Trinh, M. T.; Polak, L.; Schins, J. M.; Houtepen, A. J.; Vaxenburg, R.; Maikov, G. I.; Grinbom, G.; Midgett, A. G.; Luther, J. M.; Beard, M. C.; Nozik, A. J.; Bonn, M.; Lifshitz, E.; Siebbeles, L. D. A. Anomalous independence of multiple exciton generation on different group IV-VI quantum dot architectures. *Nano Lett.* **2011***, 11*, 1623-1629.

[17] Eisler, H.; Sundar, V. C.; Bawendi, M. G.; Walsh, M.; Smith, H. I.; Klimov, V. Color-selective semiconductor nanocrystal laser. *Appl. Phys. Lett.* **2002***, 80*, 4614-4616.

[18] Grivas, C.; Li, C.; Andreakou, P.; Wang, P.; Ding, M.; Brambilla, G.; Manna, L.; Lagoudakis, P. Single-mode tunable laser emission in the single-exciton regime from colloidal nanocrystals. *Nat. Commun.* **2013**, *4*, 2376.

[19] Philbin, J. P.; Rabani, E. Electron-Hole Correlations Govern Auger Recombination in Nanostructures. *Nano Lett.* **2018**, *18*, 7889-7895.

[20] Pietryga, J. M.; Zhuravlev, K. K.; Whitehead, M.; Klimov, V. I.; Schaller, R. D. Evidence for barrierless Auger recombination in PbSe nanocrystals: a pressure-dependent study of transient optical absorption. *Phys. Rev. Lett.* **2008**, *101*, 217401.

[21] Wang, L. W.; Califano, M.; Zunger, A.; Franceschetti, A. Pseudopotential theory of Auger processes in CdSe quantum dots. *Phys. Rev. Lett.* **2003**, *91*, 056404.

[22] Robel, I.; Gresback, R.; Kortshagen, U.; Schaller, R. D.; Klimov, V. I. Universal size-dependent trend in auger recombination in direct-gap and indirect-gap semiconductor nanocrystals. *Phys. Rev. Lett.* **2009**, *102*, 177404.

[23] Cragg, G. E.; Efros, A. L. Suppression of Auger Processes in Confined Structures. *Nano Lett.* **2010**, *10*, 313-317.

[24] Klimov, V. I. Multicarrier interactions in semiconductor nanocrystals in relation to the phenomena of Auger recombination and carrier multiplication. *Annu.Rev.Condens.Matter Phys.* **2014**, *5*, 285-316.

[25] García-Santamaría, F.; Chen, Y.; Vela, J.; Schaller, R. D.; Hollingsworth, J. A.; Klimov, V. I. Suppressed auger recombination in "giant" nanocrystals boosts optical gain performance. *Nano Lett.* **2009**, *9*, 3482-3488.

[26] Park, Y.; Lim, J.; Makarov, N. S.; Klimov, V. I. Effect of Interfacial Alloying versus "Volume Scaling" on Auger Recombination in Compositionally Graded Semiconductor Quantum Dots. *Nano Lett.* **2017**, *17*, 5607-5613.

[27] Rabouw, F. T.; Lunnemann, P.; van Dijk-Moes, R. J.; Frimmer, M.; Pietra, F.; Koenderink, A. F.; Vanmaekelbergh, D. Reduced auger recombination in single CdSe/CdS nanorods by one-dimensional electron delocalization. *Nano Lett.* **2013**, *13*, 4884-4892.

[28] Ben-Shahar, Y.; Philbin, J. P.; Scotognella, F.; Ganzer, L.; Cerullo, G.; Rabani, E.; Banin, U. Charge Carrier Dynamics in Photocatalytic Hybrid Semiconductor-Metal Nanorods: Crossover from Auger Recombination to Charge Transfer. *Nano Lett.* **2018**, *18*, 5211-5216.

[29] Cunningham, P. D.; Boercker, J. E.; Foos, E. E.; Lumb, M. P.; Smith, A. R.; Tischler, J. G.; Melinger, J. S. Enhanced multiple exciton generation in quasi-one-dimensional semiconductors. *Nano Lett.* **2011***, 11*, 3476-3481.

[30] Padilha, L. A.; Stewart, J. T.; Sandberg, R. L.; Bae, W. K.; Koh, W.; Pietryga, J. M.; Klimov, V. I. Aspect ratio dependence of auger recombination and carrier multiplication in PbSe nanorods. *Nano Lett.* **2013***, 13*, 1092-1099.

[31] Zavelani-Rossi, M.; Lupo, M. G.; Tassone, F.; Manna, L.; Lanzani, G. Suppression of biexciton Auger recombination in CdSe/CdS dot/rods: role of the electronic structure in the carrier dynamics. *Nano Lett.* **2010***, 10*, 3142-3150.

[32] Pelton, M.; Andrews, J. J.; Fedin, I.; Talapin, D. V.; Leng, H.; O'Leary, S. K. Nonmonotonic Dependence of Auger Recombination Rate on Shell Thickness for CdSe/CdS Core/Shell Nanoplatelets. *Nano Lett.* **2017***, 17*, 6900-6906.

[33] She, C.; Fedin, I.; Dolzhnikov, D. S.; Demortière, A.; Schaller, R. D.; Pelton, M.; Talapin, D. V. Low-threshold stimulated emission using colloidal quantum wells. *Nano Lett.* **2014***, 14*, 2772-2777.

[34] Li, Q.; Lian, T. Area-and thickness-dependent biexciton Auger recombination in colloidal CdSe nanoplatelets: Breaking the "universal volume scaling law". *Nano Lett.* **2017***, 17*, 3152-3158.

[35] Park, Y.; Bae, W. K.; Baker, T.; Lim, J.; Klimov, V. I. Effect of Auger recombination on lasing in heterostructured quantum dots with engineered core/shell interfaces. *Nano Lett.* **2015***, 15*, 7319-7328.

[36] Pelton, M. Carrier Dynamics, Optical Gain, and Lasing with Colloidal Quantum Wells. *J. Phys. Chem. C* **2018***, 122*, 10659-10674.

[37] Pokatilov, E. P.; Fonoberov, V. A.; Fomin, V. M.; Devreese, J. T. Electron and hole states in quantum dot quantum wells within a spherical eight-band model. *Phys. Rev. B* **2001***, 64*, 245329.

[38] Dias, E. A.; Saari, J. I.; Tyagi, P.; Kambhampati, P. Improving Optical Gain Performance in Semiconductor Quantum Dots via Coupled Quantum Shells. *J. Phys. Chem. C* **2012***, 116*, 5407-5413.

[39] Kambhampati, P.; Mack, T.; Jethi, L. Understanding and Exploiting the Interface of Semiconductor Nanocrystals for Light Emissive Applications. *ACS Photonics* **2017***, 4*, 412-423.

[40] Braun, M.; Link, S.; Burda, C.; El-Sayed, M. Transfer times of electrons and holes across the interface in CdS/HgS/CdS quantum dot quantum well nanoparticles. *Chem. Phys. Lett.* **2002***, 361*, 446-452.

[41] Xu, J.; Xiao, M. Lasing action in colloidal CdS⁄ CdSe⁄ CdS quantum wells. *Appl. Phys. Lett.* **2005***, 87*, 173117.

[42] Xu, J.; Xiao, M.; Battaglia, D.; Peng, X. Exciton radiative recombination in spherical Cd S⁄ Cd Se⁄ Cd S quantum-well nanostructures. *Appl. Phys. Lett.* **2005***, 87*, 043107.

[43] Battaglia, D.; Li, J. J.; Wang, Y.; Peng, X. Colloidal two-dimensional systems: CdSe quantum shells and wells. *Angew. Chem. Int. Ed.* **2003***, 42*, 5035-5039.

[44] Schrier, J.; Wang, L. Electronic structure of nanocrystal quantum-dot quantum wells. *Phys. Rev. B* **2006***, 73*, 245332.

[45] Schill, A. W.; Gaddis, C. S.; Qian, W.; El-Sayed, M. A.; Cai, Y.; Milam, V. T.; Sandhage, K. Ultrafast electronic relaxation and charge-carrier localization in CdS/CdSe/CdS quantum-dot quantum-well heterostructures. *Nano Lett.* **2006***, 6*, 1940-1949.

[46] Jeong, B. G.; Park, Y.; Chang, J. H.; Cho, I.; Kim, J. K.; Kim, H.; Char, K.; Cho, J.; Klimov, V. I.; Park, P. Colloidal spherical quantum wells with near-unity photoluminescence quantum yield and suppressed blinking. *ACS Nano* **2016***, 10*, 9297-9305.

[47] Xu, J.; Battaglia, D.; Peng, X.; Xiao, M. Photoluminescence from colloidal CdS-CdSe-CdS quantum wells. *J. Opt. Soc. Am. B* **2005***, 22*, 1112-1116.

[48] Braun, M.; Burda, C.; El-Sayed, M. A. Variation of the thickness and number of wells in the CdS/HgS/CdS quantum dot quantum well system. *J. Phys. Chem. A* **2001***, 105*, 5548-5551.

[49] Razgoniaeva, N.; Moroz, P.; Yang, M.; Budkina, D. S.; Eckard, H.; Augspurger, M.; Khon, D.; Tarnovsky, A. N.; Zamkov, M. One-dimensional carrier confinement in “giant” CdS/CdSe excitonic nanoshells. *J. Am. Chem. Soc.* **2017***, 139*, 7815-7822.

[50] Razgoniaeva, N.; Yang, M.; Colegrove, C.; Kholmicheva, N.; Moroz, P.; Eckard, H.; Vore, A.; Zamkov, M. Double-Well Colloidal Nanocrystals Featuring Two-Color Photoluminescence. *Chem. Mater.* **2017***, 29*, 7852-7858.

[51] Weng, C.; Chen, I.; Tsai, Y. Electron–acoustic-phonon interaction in core/shell nanocrystals and in quantum-dot quantum wells. *Phys. Rev. B* **2007***, 76*, 195313.

[52] Sippel, P.; Albrecht, W.; van der Bok, Johanna C; Van Dijk-Moes, R. J.; Hannappel, T.; Eichberger, R.; Vanmaekelbergh, D. Femtosecond cooling of hot electrons in CdSe quantum-well platelets. *Nano Lett.* **2015***, 15*, 2409-2416.

[53] Ithurria, S.; Tessier, M. D.; Mahler, B.; Lobo, R. P. S. M.; Dubertret, B.; Efros, A. L. Colloidal nanoplatelets with two-dimensional electronic structure. *Nat. Mater.* **2011***, 10*, 936-941.

[54] Ithurria, S.; Dubertret, B. Quasi 2D colloidal CdSe platelets with thicknesses controlled at the atomic level. *J. Am. Chem. Soc.* **2008***, 130*, 16504-16505.

[55] Aerts, M.; Bielewicz, T.; Klinke, C.; Grozema, F. C.; Houtepen, A. J.; Schins, J. M.; Siebbeles, L. D. A. Highly efficient carrier multiplication in PbS nanosheets. *Nat. Commun.* **2014***, 5*, 3789.

[56] Murray, C. B.; Kagan, C. R.; Bawendi, M. G. Synthesis and Characterization of Monodisperse Nanocrystals and Close-Packed Nanocrystal Assemblies. *Annu. Rev. Mater. Sci.* **2000***, 30*, 545-610.

[57] Murray, C. B.; Shevchenko, E. V.; O'Brien, S.; Talapin, D. V.; Kotov, N. A. Structural diversity in binary nanoparticle superlattices. *Nature* **2006***, 439*, 55-59.

[58] She, C.; Bryant, G. W.; Demortière, A.; Shevchenko, E. V.; Pelton, M. Controlling the spatial location of photoexcited electrons in semiconductor CdSe/CdS core/shell nanorods. *Phys. Rev. B* **2013***, 87*, 155427.

[59] Wu, K.; Lian, T. Quantum confined colloidal nanorod heterostructures for solar-to-fuel conversion. *Chem. Soc. Rev.* **2016***, 45*, 3781-3810.

[60] Razgoniaeva, N.; Yang, M.; Garrett, P.; Kholmicheva, N.; Moroz, P.; Eckard, H.; Royo Romero, L.; Porotnikov, D.; Khon, D.; Zamkov, M. Just Add Ligands: Self-Sustained Size Focusing of Colloidal Semiconductor Nanocrystals. *Chem. Mater.* **2018***, 30*, 1391-1398.

[61] Kholmicheva, N.; Yang, M.; Moroz, P.; Eckard, H.; Vore, A.; Cassidy, J.; Pushina, M.; Boddy, A.; Porotnikov, D.; Anzenbacher, P.; Zamkov, M. Ion-Mediated Ligand Exchange and Size-Focusing Of Semiconductor Nanocrystals in Ligand-Saturated Solutions. *J. Phys. Chem. C* **2018**, *122*, 23623-23630.

[62]Mooney, J.; Krause, M. M.; Saari, J. I.; Kambhampati, P. Challenge to the deep-trap model of the surface in semiconductor nanocrystals. *Phys. Rev. B* **2013***, 87*, 081201.

[63] Cirillo, M.; Aubert, T.; Gomes, R.; Van Deun, R.; Emplit, P.; Biermann, A.; Lange, H.; Thomsen, C.; Brainis, E.; Hens, Z. "Flash" Synthesis of CdSe/CdC Core–Shell Quantum Dots. *Chem. Mater.* **2014**, *26*, 1154-1160.

[64] Sewall, S. L.; Cooney, R. R.; Anderson, K. E.; Dias, E. A.; Kambhampati, P. State-to-state exciton dynamics in semiconductor quantum dots. *Phys. Rev. B* **2006**, *74*, 235328.

[65] Houtepen, A. J.; Vanmaekelbergh, D. Orbital occupation in electron-charged CdSe quantum-dot solids. *J. Phys. Chem. B* **2005**, *109*, 19634-19642.

[66] Sacra, A.; Norris, D. J.; Murray, C. B.; Bawendi, M. G. Stark spectroscopy of CdSe nanocrystallites: The significance of transition linewidths. *J. Chem. Phys.* **1995**, *103*, 5236-5245.

[67] Huang, J.; Huang, Z.; Yang, Y.; Zhu, H.; Lian, T. Multiple exciton dissociation in CdSe quantum dots by ultrafast electron transfer to adsorbed methylene blue. *J. Am. Chem. Soc.* **2010**, *132*, 4858-4864.

[68] Klimov, V. I.; Mikhailovsky, A. A.; McBranch, D. W.; Leatherdale, C. A.; Bawendi, M. G. Quantization of multiparticle Auger rates in semiconductor quantum dots. *Science* **2000**, *287*, 1011-1013.

[69] Kong, D.; Jia, Y.; Ren, Y.; Xie, Z.; Wu, K.; Lian, T. Shell-Thickness-Dependent Biexciton Lifetime in Type I and Quasi-Type II CdSe@ CdS Core/Shell Quantum Dots. *J. Phys. Chem. C* **2018**, *112*, 14091-14098.

[70] Htoon, H.; Hollingsworth, J. A.; Dickerson, R.; Klimov, V. I. Effect of zero-to one-dimensional transformation on multiparticle auger recombination in semiconductor quantum rods. *Phys. Rev. Lett.* **2003**, *91*, 227401.

[71] Klimov, V. I.; Ivanov, S. A.; Nanda, J.; Achermann, M.; Bezel, I.; McGuire, J. A.; Piryatinski, A. Single-exciton optical gain in semiconductor nanocrystals. *Nature* **2007**, *447*, 441-446.

[72] Oron, D.; Kazes, M.; Banin, U. Multiexcitons in type-II colloidal semiconductor quantum dots. *Phys. Rev. B* **2007**, *75*, 035330.

[73] Yu, W. W.; Peng, X. Formation of high-quality CdS and other II-VI semiconductor nanocrystals in noncoordinating solvents: Tunable reactivity of monomers. *Angew. Chem. Int. Ed.* **2007**, *46*, 2559-2559.

[74] Jeong, B. G.; Park, Y.; Chang, J. H.; Cho, I.; Kim, J. K.; Kim, H.; Char, K.; Cho, J.; Klimov, V. I.; Park, P.; Lee, D. C.; Bae, W. K. Colloidal Spherical Quantum Wells with Near-Unity Photoluminescence Quantum Yield and Suppressed Blinking. *ACS Nano* **2016***, 10*, 9297-9305.

[75] Kovalenko, S. A.; Dobryakov, A. L.; Ruthmann, J.; Ernsting, N. P. Femtosecond spectroscopy of condensed phases with chirped supercontinuum probing. *Phys. Rev. A* **1999***, 59*, 2369-2384.